A R C H I V E S O F M E T A L L U R G Y A N D M A T E R I A L S
Volume 59 2014 Issue 4
DOI: 10.2478/amm-2014-0283

A. GRAJCAR*, A. KILARSKI**, K. RADWAŃSKI***, R. SWADŹBA***

MICROSTRUCTURAL FEATURES OF STRAIN-INDUCED MARTENSITIC TRANSFORMATION IN MEDIUM-Mn STEELS WITH METASTABLE RETAINED AUSTENITE

CECHY MIKROSTRUKTURALNE INDUKOWANEJ ODKSZTAŁCENIEM PRZEMIANY MARTENZYTYCZNEJ W STALACH ŚREDNIOMANGANOWYCH Z METASTABILNYM AUSTENITEM SZCZĄTKOWYM

The work addresses relationships between the microstructure evolution and mechanical properties of two thermomechanically processed bainitic steels containing 3 and 5% Mn. The steels contain blocky-type and interlath metastable retained austenite embeded between laths of bainitic ferrite. To monitor the transformation behaviour of retained austenite into strain-induced martensite tensile tests were interrupted at 5%, 10%, and rupture strain. The identification of retained austenite and strain-induced martensite was carried out using light microscopy (LM), scanning electron microscopy (SEM) equipped with EBSD (Electron Backscatter Diffraction) and transmission electron microscopy (TEM). The amount of retained austenite was determined by XRD. It was found that the increase of Mn addition from 3 to 5% detrimentally decreases a volume fraction of retained austenite, its carbon content, and ductility.

Keywords: multiphase steel, medium-Mn steel, TRIP effect, strain-induced martensite, retained austenite, carbide-free bainite

W pracy przedstawiono zależności pomiędzy rozwojem mikrostruktury i własnościami mechanicznymi dwóch obrobionych cieplno-plastycznie stali bainitycznych zawierających 3 i 5% Mn. Stale zawierają blokowe ziarna i warstwy austenitu szczątkowego umieszczone pomiędzy listwami ferrytu bainitycznego. W celu monitorowania postępu przemiany austenitu szczątkowego w martenzyt odkształceniowy, próby rozciągania prowadzono do zerwania oraz przerywano przy odkształceniu 5 i 10%. Identyfikacji austenitu szczątkowego oraz martenzytu odkształceniowego dokonano przy użyciu mikroskopii świetlnej (LM), skaningowej mikroskopii elektronowej (SEM) z wykorzystaniem techniki EBSD (Electron Backscatter Diffraction), a także transmisyjnej mikroskopii elektronowej (TEM). Udział austenitu szczątkowego wyznaczono metodą rentgenowską. Stwierdzono, że wzrost zawartości Mn z 3 do 5% obniża udział austenitu szczątkowego, stężenie węgla w tej fazie, a także ciągliwość stali.

1. Introduction

Strain-induced martensitic transformation of retained austenite resulting in additional plasticity and improved formability of steel sheets has been successfully utilized in TRIP-aided multiphase steels containing ferrite, bainite and retained austenite [1-3]. Transformation-induced plasticity (TRIP) and Twinning-induced plasticity (TWIP) effects are major sources of a superior balance between strength and plasticity in high-manganese austenitic alloys [4-8]. Recently, the automotive industry searches for cost-efficient steel sheets showing a mechanical properties regime between conventional multiphase steels and high-alloyed manganese steels. These requirements can be met by a third generation of advanced high-strength steels including medium-Mn steels, quenching and partitioning (QP) approaches, nano-bainitic alloys etc [9-15].

At present, one of the most advanced approach is focused on medium-Mn steels (3-12 wt.%) produced by intercritical annealing of cold-rolled low-carbon martensitic steel sheets. These steels belong to ultra-fine grained ferritic-austenitic alloys. The retention of a large volume fraction of γ phase at room temperature is obtained due to carbon and manganese partitioning during annealing and grain refinement [9, 10, 12, 13]. All the factors decrease martensite start temperature effectively but manganese partition from ferrite into austenite upon the intercritical annealing requires long austenitizing times. Another manufacturing concept applied for medium-Mn steels includes thermomechanically processed steel sheets produced by a multi-step cooling following hot rolling [11]. This concept requires an austempering step at a bainitic transformation range to enrich austenite in carbon. The acceleration of the bainitic transformation kinetics can be ensured by aluminium

* SILESIAN UNIVERSITY OF TECHNOLOGY, INSTITUTE OF ENGINEERING MATERIALS AND BIOMATERIALS, 18A KONARSKIEGO STR., 44-100 GLIWICE, POLAND
** GENERAL MOTORS MANUFACTURING POLAND, 1 ADAMA OPLA STR., 44-121 GLIWICE, POLAND
*** INSTITUTE FOR FERROUS METALLURGY, 12-14 K. MIARKI STR., 44-100 GLIWICE, POLAND

addition in contrast to Si-bearing steels, which use require long austempering times [16, 17].

Mechanical properties and formability of multiphase steels are mainly dependent on mechanical stability of retained austenite upon cold deformation. It is generally known that a blocky retained austenite is transformed into martensite at an initial stage of straining [1-3]. The microstructure of medium-Mn steels, nano-bainite and QP steels contains predominantly lamellar or nano-scale retained austenite characterized by increased mechanical stability when compared to the blocky grains [10, 12, 13, 18, 19]. However, its mechanical stability is strongly dependent on a C-Mn ratio, lamella's thickness, dislocation density, a microstructural neighbour etc [20,21]. At present, relationships between mechanical behaviour and microstructure are mainly investigated in cold-rolled medium-Mn steels. Therefore, the aim of the present work is to shed some light on strain-induced martensitic transformation in thermomechanically processed medium-Mn steels containing metastable lamellar retained austenite.

2. Experimental procedure

The chemical composition of new-developed vacuum-melted medium-Mn steels is given in Table 1. The difference in Mn content is the basis for steel designation (3MnAl, 5MnAl). Mn was used to stabilize austenite whereas the low-Si – high-Al approach was chosen to obtain carbide-free bainite. Molybdenum was used to increase a strength level. The ingots were hot-forged and roughly rolled to a thickness of about 9 mm. Thermomechanical processing consisted of hot rolling of flat samples in 5 passes to a final thickness of 3.3 mm obtained at the finishing rolling temperature of 750°C. Next, the 3MnAl sheet samples were slowly cooled within 5 s to 700°C followed by the controlled mixed air-blow and water-spray cooling to an austempering temperature of 400°C. The isothermal holding time was 300 s. The 5MnAl steel samples were directly cooled to 400°C following finishing rolling.

TABLE 1
Chemical composition of the investigated steels (wt. %)

Steel designation	C	Mn	Al	Si	Mo	S	P
3MnAl	0.17	3.3	1.7	0.22	0.23	0.014	0.010
5MnAl	0.16	4.7	1.6	0.20	0.20	0.004	0.008

Tensile test samples with a gauge length of 50 mm were cut parallel to the rolling direction of sheets. The static tensile test was carried out at a strain rate of 5×10^{-3} s^{-1}. Interrupted tensile tests were carried out to monitor strain-induced transformation of retained austenite as a function of strain. The tests were interrupted at different tensile strain in steps of 5%. Metallographic specimens were taken along the tensile direction. For a microstructural analysis, methods of LM, SEM, and TEM were used. The orientation imaging microscopy (OIM) using SEM was also applied.

Morphological details of microstructural constituents were revealed with the SUPRA 25 SEM using back-scattered electrons (BSE). Observations were performed on nital-etched samples at the accelerating voltage of 20kV. The EBSD technique was performed by the use of the Inspect F SEM equipped with Shottky's field emission. After classical grinding and polishing, specimens were polished with Al_2O_3 with granularity of 0.1 μm. The final step of sample preparation was their ion polishing using GATAN 682 PECS system.

Thin foils investigations were carried out by the use of the JEOL JEM 3010 at the accelerating voltage of 200 kV. Mechanically grinded disk specimens were polished at the voltage of 17 V and current density of 0.2 A/cm^2. The mixture of 490 ml H_3PO_4+ 7 ml H_2SO_4+ 50g CrO_3 was used as the electrolyte. Determination of retained austenite volume fraction and its carbon content were performed using X-ray phase analysis basing on the Rietveld method. X-ray investigations were done using an X-pert PRO diffractometer equipped with an X'Celerator detector and Co radiation. The positions of maxima of the diffractions lines of austenitic phase were used to determine the lattice constant of austenite a_γ. This parameter is necessary to calculate the carbon content in retained austenite (C_γ). The following formula was used [22]:

$$a_\gamma = 0.3578 + 0.0033C_\gamma \quad (1)$$

where a_γ is the lattice parameter of retained austenite (nm).

3. Results and discussion

Initial microstructures obtained as a result of the thermomechanical processing are characterized by substantial grain refinement. It is due to strong deformation of prior austenite and resulting numerous places for nucleation of lath transformation products. The micrograph in Fig. 1 shows the typical microstructure of the 3MnAl steel consisting of bainitic ferrite laths containing blocky grains and interlath retained austenite (Fig. 1a). A fraction of polygonal ferrite is very small because of high hardenability of steel. At the larger magnification it is revealed that totally stable is only interlath retained austenite (Fig. 1b). This type of microstructure with carbides replaced by layers of retained austenite is called carbide-free bainite [3, 9, 10]. Blocky austenite grains larger than about 2 μm transformed upon cooling to room temperature forming martensite-austenite (M-A) constituents. Interlath retained austenite is a major morphological type of γ phase in the steel containing a higher Mn content. It is located between bainitic ferrite laths forming bainitic-austenitic (B-A) constituents (Fig. 2). Some blocky grains are partially transformed into martensite forming M-A constituents.

It is clearly seen that the amount of retained austenite is higher in the 3MnAl steel than in the 5MnAl steel when Figs. 1 and 2 are compared. It is confirmed by XRD results. The volume fraction of γ phase is equal to 17.7% for the 3MnAl steel whereas it decreases to 9.6% for the steel containing 5% Mn. This difference is strictly related to the carbon concentrations in retained austenite amounting to 1.22 wt.% and 1.04 wt.%. – respectively for the 3MnAl and 5MnAl steels. The C content in retained austenite in carbide-free bainitic steels is determined by T_0 temperature, where austenite and ferrite of the same composition have identical free energies [17, 23]. According to Takahashi and Bhadeshia [23] manganese reduces the T_0 temperature and a resulting C content

in γ phase. Results of Sugimoto et al. [24] confirmed that the C concentration in retained austenite decreased from 1.53 to 1.13% with increasing the Mn content from 1 to 2.5%. The increased Mn content in the present work (3% and 5%) results in the lowered C content in retained austenite revealing as the occurrence of M-A constituents in the initial microstructure.

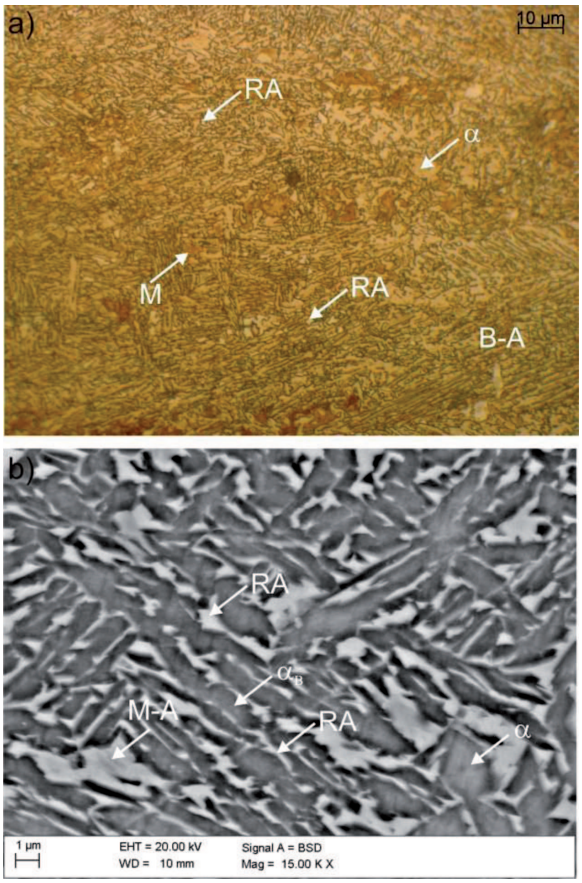

Fig. 1. Microstructure of the thermomechanically processed 3MnAl steel containing bainitic ferrite laths (α_B), retained austenite (RA), polygonal ferrite (α), and martensite-austenite (M-A) constituents; LM (a), SEM (b)

At 5% strain the amount of retained austenite in the 3MnAl steel decreases from 17.7% to about 10%. The evidence of the strain-induced martensitic transformation at 5% strain is the SEM micrograph in Fig. 3a. It can be clearly observed that the strain-induced martensite forms in the blocky grains of retained austenite. On the other hand, interlath retained austenite is untransformed. Under rupture conditions near a total volume fraction of blocky retained austenite transformed into strain-induced martensite (Fig. 3b). However, boundary regions of austenite grains and interlath retained austenite are mechanically stable. These regions have better conditions to be enriched in C when compared to a center of grains because of shorter diffusion path of carbon.

Very useful quantitative results on morphological details of the multiphase microstructure can be obtained analyzing EBSD images. Figure 4 shows EBSD maps registered at 5% strain for the 3MnAl steel. Comparing the image quality (IQ) map (Fig. 4a) and phase map (Fig. 4b) it is possible to identify particular structural constituents. In the grey scale IQ map retained austenite regions correspond to the dark areas of the

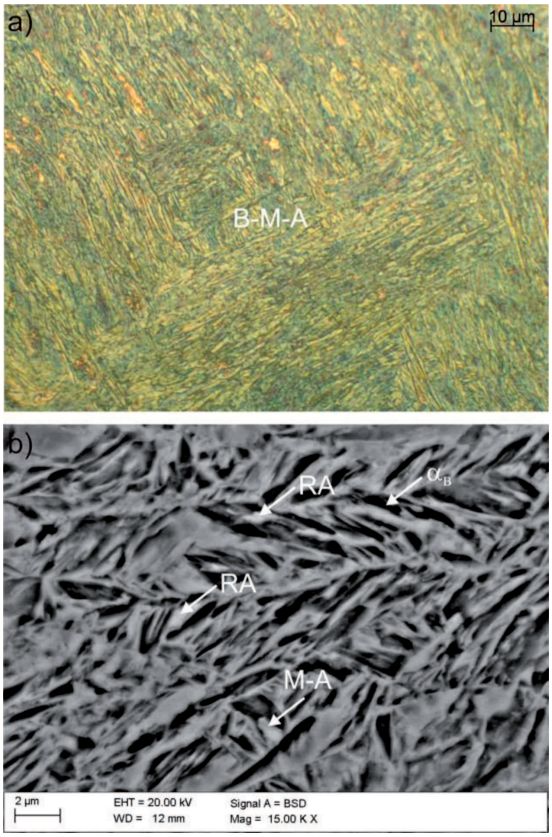

Fig. 2. Microstructure of the thermomechanically processed 5MnAl steel containing bainitic ferrite laths (α_B), retained austenite (RA), and martensite-austenite (M-A) constituents; LM (a), SEM (b)

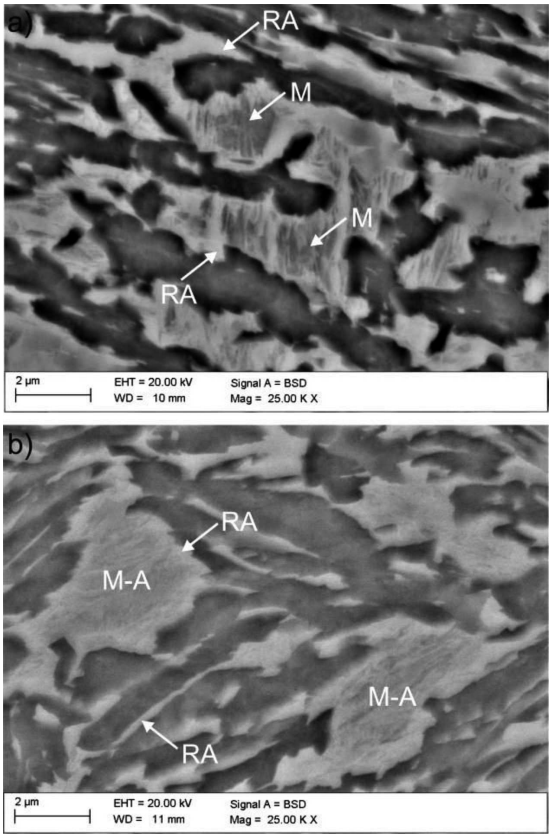

Fig. 3. Strain-induced martensite (M), martensite-austenite (M-A) islands and retained austenite (RA) in the microstructure of the 3MnAl steel cold deformed to 5% strain (a), and to 14.8% strain – rupture of the sample (b)

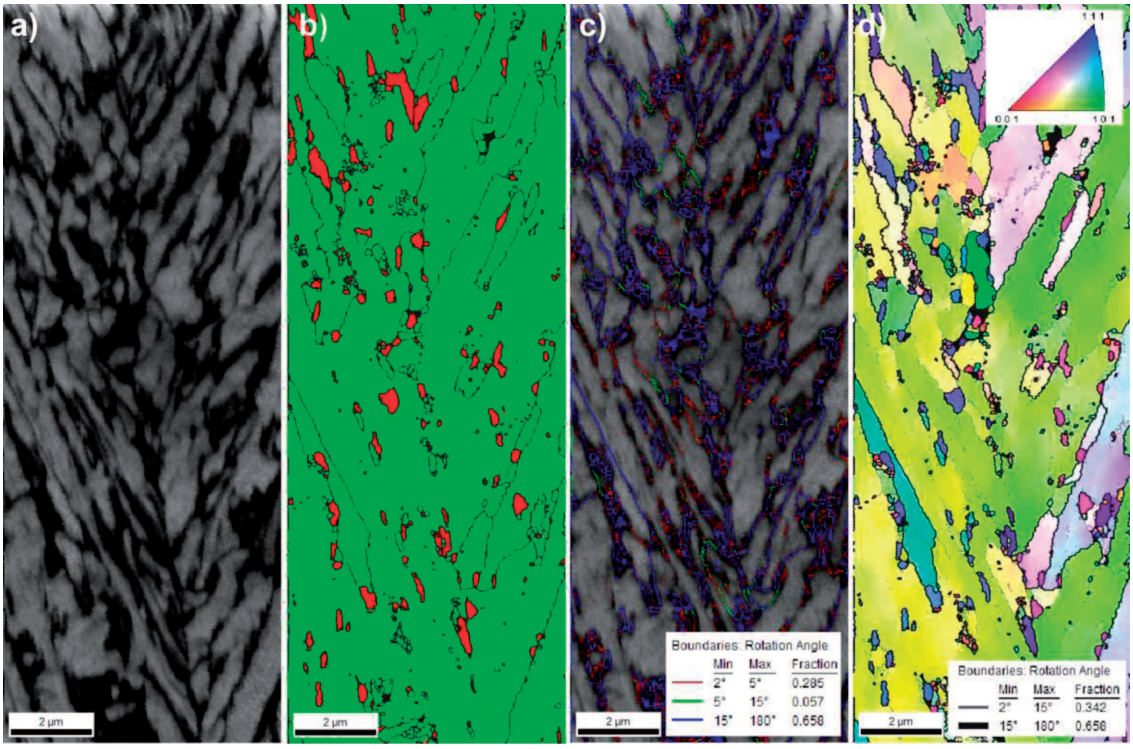

Fig. 4. Image quality (IQ) map (a), phase map showing retained austenite in red (b), IQ map with misorientation angles (c), and inverse pole figure map with low-angle (2°-15°) and high-angle (15°-180°) boundaries registered at 5% strain for the 3MnAl steel

poor diffraction quality. The IQ factor represents a quantitative description of the sharpness of the EBSD pattern. A lattice distorted by crystalline defects such as dislocations and grain/subgrains boundaries has a distorted Kikuchi pattern leading to lower IQ values [2, 25]. Hence, strain-induced martensite can be distinguished from bainitic ferrite because it is the most defected phase and thus it shows the worst diffraction quality. The retained austenite marked in the phase map (Fig. 4b) is strongly fragmented due to a progress of martensitic transformation. A majority of the blocky grains transformed partially into martensite.

It should be noted that the number fraction of misorientation angles lower than 5° is close to 30% (Fig. 4c). It is the evidence of advancing the dislocation substructure [2, 25] being a result of a low finishing rolling temperature of 750°C and transformation texture [26]. The inverse pole figure map in Fig. 4d indicates that a majority of BCC constituents show a <101>microtexture whereas retained austenite is preferentially oriented along a <111>direction.

The EBSD technique does not allow detecting smallest particles of retained austenite because of its limited resolution. It can only be done using TEM. Figure 5 shows TEM micrographs of the 3MnAl steel registered at 5% strain (Fig. 5a) and at 10% strain (Fig. 5b). It is clear that some nanoscale particles are mechanically unstable and they transform into strain-induced martensite (M). The formed martensite has a plate morphology, what confirms that it is created from a high-carbon austenite. Boundary regions of γ phase layers remain still untransformed.

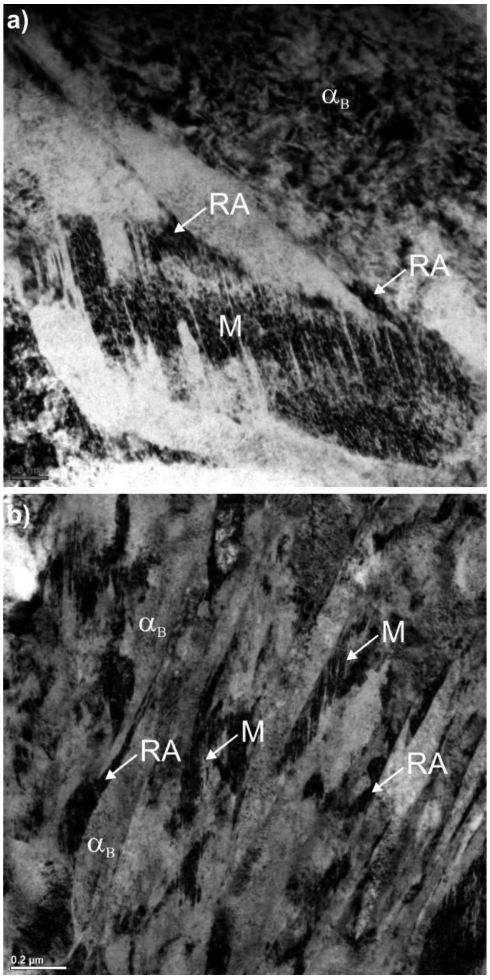

Fig. 5. TEM micrographs showing strain-induced martensite (M), retained austenite (RA), and bainitic ferrite laths (α_B) of the 3MnAl steel at 5% strain (a) and 10% strain (b)

TABLE 2
Mechanical properties of the investigated steels

Steel code	$YS_{0.2}$, MPa	UTS, MPa	TEl, %
3MnAl	684	986	14.8
5MnAl	901	1259	8.0

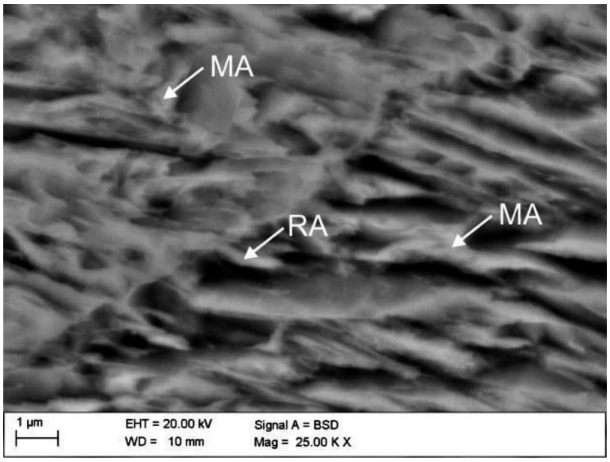

Fig. 6. Martensite-austenite (M-A) constituents and interlath retained austenite (RA) in the microstructure of the 5MnAl steel cold deformed to 5% strain

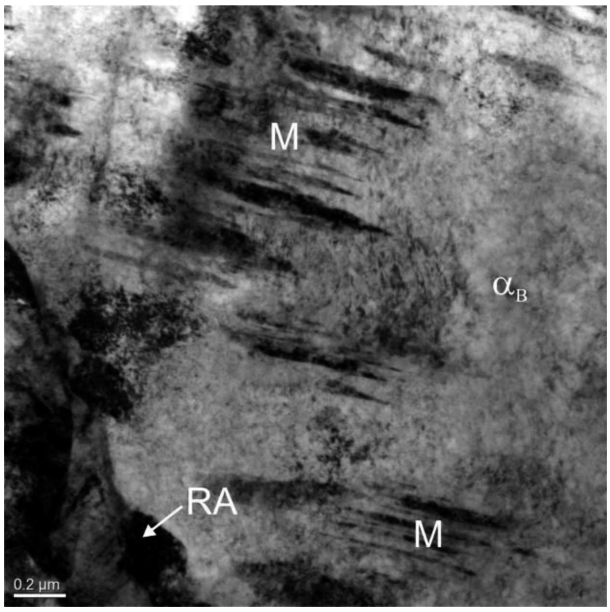

Fig. 7. TEM micrograph showing strain-induced martensite (M), retained austenite (RA), and bainitic ferrite (α_B) of the 5MnAl steel at 5% strain

Results of mechanical properties listed in Table 2 indicate that a high strength level ($YS_{0.2}$ ~700 MPa, UTS ~1000 MPa) at reasonable ductility (TEl ~15%) can be obtained in the 3MnAl steel. It is due to a gradual martensitic transformation of blocky retained austenite grains and a partial transformation of γ phase layers located between bainitic ferrite laths. Significantly higher strength properties shows the 5MnAl steel with a UTS level above 1250 MPa. However, retained austenite has the low mechanical stability and it transforms intensively into martensite even at 5% strain forming numerous M-A constituents (Fig. 6). It is confirmed by a TEM micrograph in Fig. 7 showing plate martensite and small areas of retained austenite located at grain boundaries. The strong work strengthening at the initial stage of cold working results in premature rupture of the specimen at the TEl = 8%. The low stability of retained austenite layers in the 5MnAl steel is due to the relatively low C enrichment of retained austenite (C_γ = 1.04 wt.%.).

4. Conclusion

The evolution of the microstructure as a function of increasing strain was monitored in two thermomechanically processed medium-Mn steels. It was found that the 3MnAl steel contains a higher volume fraction of retained austenite (17.7%) than the steel containing 5% Mn (9.6%). Retained austenite of the steel with 3% Mn is also more enriched in carbon. Strain-induced martensite forms initially in blocky γ grains and then the martensitic transformation is initiated in retained austenite located between bainitic ferrite laths. At rupture conditions mechanically stable are retained austenite films and boundary regions of blocky grains strongly fragmented by formed plate martensite. Increase of Mn content to 5% affects detrimentally the mechanical stability of γ phase. Layers of this phase are easily transformed into martensite even at 5% strain leading to strong strengthening and premature fracture (TEl = 8%). Metastable retained austenite is transformed in a more gradual way in the 3MnAl steel. It allows obtaining TEl = 14.8% at UTS close to 1000 MPa.

REFERENCES

[1] S. Zaefferer, J. Ohlert, W. Bleck, Acta Mater. **52**, 2765 (2004).
[2] R. Petrov, L. Kestens, A. Wasilkowska, Y. Houbaert, Mater. Sci. Eng. A **447**, 285 (2007).
[3] Y.F. Shen, Y.D. Liu, X. Sun, Y.D. Wang, L. Zuo, R.D.K. Misra, Mater. Sci. Eng. A **583**, 1 (2013).
[4] S. Lasek, E. Mazancova, Metalurgija **52**, 4, 441 (2013).
[5] A. Grajcar, M. Opiela, G. Fojt-Dymara, Arch. Civ. Mech. Eng. **9**, 49 (2009).
[6] Z. Muskalski, S. Wiewiórowska, M. Pełka, Solid State Phenom. **199**, 525 (2013).
[7] L.A. Dobrzanski, W. Borek, Arch. Civ. Mech. Eng. **12**, 299 (2012).
[8] D. Kuc, E. Hadasik, G. Niewielski, I. Schindler, E. Mazancova, S. Rusz, P. Kawulok, Arch. Civ. Mech. Eng. **12**, 3, 312 (2012).
[9] P.J. Gibbs, E. De Moor, M.J. Merwin, B. Clausen, J.G. Speer, D.K. Matlock, Metall. Mater. Trans. A **42**, 3691 (2011).
[10] S.-J. Lee, S. Lee, B.C. De Cooman, Scripta Mater. **64**, 649 (2011).
[11] A. Grajcar, S. Lesz, Mater. Sci. Forum **706-709**, 2124 (2012).
[12] J. Shi, X. Sun, M. Wang, W. Hui, H. Dong, W. Cao, Scripta Mater. **63**, 815 (2010).
[13] C. Wang, J. Shi, C.Y. Wang, W.J. Hui, M.Q. Wang, ISIJ Int. **51**, 651 (2011).

[14] H. Jirkova, B. Masek, M.F.X. Wagner, D. Langmajerova, L. Kucerova, R. Treml, D. Kiener, J. Alloys Comp. (2013), doi.org/10.1016/j.jallcom.2013.12.028.
[15] F.G. Caballero, C. Garcia-Mateo, J. Chao, M.J. Santofimia, C. Capdevila, C.G. de Andres, ISIJ Int. **48**, 1256 (2008).
[16] K. Sugimoto, B. Yu, Y. Mukai, S. Ikeda, ISIJ Int. **45**, 1194 (2005).
[17] C. Garcia-Mateo, F.G. Caballero, H.K.D.H. Bhadeshia, ISIJ Int. **43**, 1821 (2003).
[18] P. Pawluk, E. Skołek, M. Kopcewicz, W. Świątnicki, Solid State Phenom. **203-204**, 150 (2013).
[19] S.-J. Lee, S. Lee, B.C. De Cooman, Int. J. Mater. Res. **104**, 423 (2013).
[20] A. Kokosza, J. Pacyna, Arch. Metall. Mater. **59**, 1017 (2014).
[21] M.B. Jabłońska, Arch. Metall. Mater. **59**, 1193 (2014).
[22] Z.C. Wang, S.J. Kim, C.G. Lee, T.H. Lee, J. Mater. Proc. Tech. **151**, 141 (2004).
[23] M. Takahashi, H.K.D.H. Bhadeshia, Mater. Trans. JIM. **32**, 689 (1991).
[24] K. Sugimoto, N. Usui, M. Kobayashi, S. Hashimoto, ISIJ Int. **32**, 1311 (1992).
[25] A.J. DeArdo, C.I. Garcia, K. Chuo, M. Hua, Mater. Manuf. Proc. **25**, 33 (2010).
[26] A. Lambert-Perlade, A.F. Gourgues, A. Pineau, Acta Mater. **52**, 2337 (2004).

Received: 20 October 2013.